water

MDPI

Article

Zeolite Adsorbents for Selective Removal of Co(II) and Li(I) from Aqueous Solutions

Eduardo Díez *, Cinthya Redondo, José María Gómez, Ruben Miranda and Araceli Rodríguez

Chemical and Materials Engineering, Complutense University of Madrid, Avda. Complutense S/N, 28040 Madrid, Spain

* Correspondence: ediezalc@ucm.es; Tel.: +34-91-394-8509

Abstract: Cobalt and lithium are critical metals because of its shortage, difficulty of extraction and huge economic impact due to their market value. The purpose of this work is to study their selective removal from aqueous solutions in different conditions using two commercial FAU zeolites as adsorbent materials. These solids were characterized by XRD, XRF and BET analysis, to follow up of their FAU structure integrity, their Si/Al ratio, and their specific surface area evolutions through their preparation process. The kinetic study indicates that using both zeolites with a dosage of 5 g/L a 100% cobalt removal from aqueous solutions is achievable, while lithium removal is kept around 30% (separation factor of 3.33). This selectivity is important as these two metals frequently appear together in leaching solutions form, for example, ion-Li batteries. In relation to the adsorption equilibrium, cobalt adsorption presents a finite adsorption capacity while this behavior is not observed in lithium adsorption. For this reason, Langmuir model is the most adequate to represent cobalt adsorption, while lithium adsorption is better represented by Freundlich model.

Keywords: zeolite X and Y; cobalt; nickel and lithium cations; critical metals; adsorption kinetics and isotherms; thermodynamic parameters

Citation: Díez, E.; Redondo, C.; Gómez, J.M.; Miranda, R.; Rodríguez, A. Zeolite Adsorbents for Selective Removal of Co(II) and Li(I) from Aqueous Solutions. *Water* **2023**, *15*, 270. https://doi.org/10.3390/w15020270

Academic Editors: Sílvia Santos, Antonio Turco and Ariana Pintor

Received: 8 December 2022
Revised: 31 December 2022
Accepted: 6 January 2023
Published: 9 January 2023

1. Introduction

Nowadays, a large environmental problem exists due to heavy metal ions are present in the environment, and they are considered as the most widespread toxic mineral contaminants of soil and water systems. The main problem of these ions is that they are non-biodegradable and tend to accumulate in living organisms, causing different diseases and disorders [1].

Heavy metal ions come to water systems from two ways: natural ones, which include volcanic activities and soil and mineral erosion, and anthropogenic ones, that comprise mineral processing, fuel combustion, agricultural and industrial activities, especially those derived from wastes of the electronic, electroplating, and petrochemical industries [1–5].

Apart from the importance of removing these contaminants from water, their recovery is also becoming essential, because most of them are critical metals due to their scarcity and wide range of applications. Among them, cobalt and lithium are largely used in catalysis, alloys, steels, batteries, semi-conductors and much more applications [5–10]. In fact, according to the last European Commission report on critical raw materials [11], cobalt and lithium are considered to be critical.

The removal of Co(II) and Li(I) ions from large volumes of wastewater can be carried out by various conventional methods such as chemical precipitation [5], solvent extraction [12], membrane filtration [13], ion exchange [1], electrochemical removal [14] or coagulation [15]. However, many of these techniques involve some disadvantages such as incomplete removal, high-energy requirements and toxic sludge production, low efficiency, sensitive operating conditions, costly disposal and not being suitable for small-scale industries [3,7,8]. Consequently, the most suitable method for ion removal and pre-concentration

from aqueous solutions is adsorption, mostly because is highly effective, even at low concentrations, and is cheaper than other methods, mainly because of the mild operation conditions [3,16]. Adsorption is a surface phenomenon involving the accumulation of solute species from an aqueous solution onto a substrate surface. In literature, adsorption has been successfully employed to remove silver [17], cadmium [18], arsenic [19], antimony [20], or uranium ions [21].

Concerning cobalt adsorption from aqueous solutions, Prabakaran and Arivoli [22] studied the preparation of activated carbon from Thespesia populnea bark as a low cost biosorbent, Kobya et al. [23] used activated carbon prepared from apricot stone, and Deravanesiyan et al. [24] focused their study on the synthesis of alumina nanoparticles immobilized zeolite by sol-gel and physical methods.

In relation to lithium adsorption, Lemaire et al. [4] evaluated lithium separation from aqueous solutions using Amberlite IR 120 resin and molecular sieve 13X. At this point it is important to emphasize that these two ions frequently appear together in aqueous media, after the leaching of end-of-life lithium-ion batteries [25].

On the other hand, as well as the adsorption, the desorption process of these ions for their recovery is also important. Although it is true that an adsorption/desorption cycle does not allow directly recovering the metal ions, it allows their pre-concentration. This fact is key factor for the further recovery by other techniques. Additionally, in many cases, desorption takes place by means of acidic solutions. Although, at first sight, it would seem to be a drawback, however, considering that many operations employed to recover metal ions from pre-concentrated aqueous solutions imply acidic conditions, this fact should not involve an additional difficulty. As an example, a previous study of the authors [26], focused on the synthesis of a mesoporous activated carbon as adsorbent to pre-concentrate indium from aqueous solution and recover it, employed a solution of HNO_3 (pH = 0.5). However, the use of nitric can alter the surface of the carbon, which is an important factor if the cost of the adsorbent is relatively high. Additionally, the recovery of lithium from an aqueous solution by sorption/desorption method was studied by Lemaire et al. [4].

One of the factors that mainly influences the adsorption process is the nature of the adsorbent. In a way, the relatively low cost of the adsorption technique is closely related to the cost of the adsorbent. In addition, the adsorption/desorption processes of Co(II) and Li(I) ions in the solid adsorbents is closely related to its mobility [3] so, in order to design an adequate adsorption system, it is fundamental to try out different adsorbent materials with different physical and chemical properties. In this sense, several researchers have previously tried different materials to treat aqueous systems polluted with metals. As an example, Li et al. [27] synthetized a zeolite-activated carbon composite as an adsorbent for the removal of heavy metal ions and macromolecular organics. A recent review of the different materials employed as adsorbents to remove metal from aqueous solutions was published by Iftekhat et al. [28].

The aim of this study is to test different adsorbent materials to obtain the most favorable adsorbent to recover Co(II) and Li(I) ions of aqueous solutions. The final purpose is to design a system to selectively separate the two ions as they frequently appear together in aqueous solutions coming from e-wastes and they belong to critical raw materials group, according to the European Commission [11]. To achieve this purpose, their kinetic, thermodynamic and isotherm data are extremely important. Among the potential adsorbents, zeolites have been selected because they have successfully employed to remove metals from aqueous media [29], as well as they are relatively affordable solids.

2. Materials and Methods

2.1. Materials

$Co(NO_3)_2{\cdot}6H_2O$ purchased from Sigma Aldrich (St. Louis, MO, USA) and LiCl purchased from Alfa Aesar (Ward Hill, MA, USA), were employed as the source of Cobalt (II) and Lithium (I), respectively.

Two zeolites were employed as adsorbents, 13XBFK, zeolite X type, and NaYBFK, zeolite Y type, supplied by Chemiewerk Bad Köstritz GmbH (CWK) (Bad Köstritz, Germany). These zeolites were also used in their protonated form, 13XBFK(H) and NaYBFK(H), with the purpose of improving the adsorption process by exchanging the cations with protons in the zeolite [30]. The ion-exchange of X and Y zeolites was performed following this three-step procedure: first, the solids were washed 5 times the solids with a 0.005 M HCl solution, employing 10 mL of solution per gram of zeolite; second, the solids were washed 5 times with MilliQ water; and finally, the solids were dried at 383 K. In previous references it was checked that a diluted HCl solution was equally effective than employing ammonium to protonate the zeolite [30].

To characterize the solid materials used in this study, different techniques were employed. Adsorption–desorption isotherms of N_2 at 77 K were carried out using an ASAP 2020 Micromeritics (Norcross, GA, USA) adsorption analyzer, in a p/p_0 range from 0 to 1. The specific surface area (SBET) was determined employing the standard Brunauer–Emmett–Teller (BET) method. Additionally, external surface area (SEXT) was determined using t-plot method, and pore size distribution (PSD) curves were calculated by the BJH (Barrett–Joyner–Halenda) method with the KJS (Kruk–Jaroniec–Sayari) correction.

X-ray diffraction (XRD) was employed to examine the crystal structure of zeolites. The measurements were performed in a PANalytical X'Pert MPD (Malvern, UK) using a CuKα radiation in the range of 5–70°, and with a step size of 0.1°. X-ray fluorescence (XRF) was employed to determine the chemical composition. The measurements were carried out using an Aχios PANalytical apparatus (Malvern, UK).

Furthermore, Fourier Transform Infrared Spectroscopy (FTIR) measurements were carried out by a Thermo Nicolet FT-IR (Thermo Fisher, Waltham, MA, USA). The samples were scanned in the range of 4000–400 cm^{-1} and the band intensities were expressed in transmittance.

Finally, the pH evolution of the solid suspensions was evaluated by placing a solid dosage of 1 g/L of the different materials in Eppendorf tubes. Afterwards, the Eppendorf tubes were located in a thermo block (Optic Ivymen System; Biotech, Barcelona, Spain) apparatus, to provide orbital agitation and to maintain constant temperature. Finally, the pH was measured at different times with a Crison (Barcelona, Spain) micro pH 2002 apparatus.

2.2. Adsorption Kinetic Experiments

The adsorption kinetic experiments were carried out in batch using tubes (25 mL sample) placed in a thermo block (Hettich Lab Technology; Tuttlingen, Germany), stirred at 1100 rpm, at 298 K. The experimental procedure was carried out as follows: initially, the appropriate dosage of the adsorbent was added to a tube containing a metal aqueous solution with the desired Co(II) or Li(I) concentration. Then, the tube was placed in the stirring block and was agitated at constant temperature until the adsorption test was finished. Once the adsorption experiment had ended, to completely ensure the absence of solids in the analysis spectrophotometer, the adsorbent was separated from the aqueous solution by centrifugation (11,000 rpm) using a Spectrafuge 24D from Labnet International, Inc. (Edison, NJ, USA) apparatus, and subsequently filtered with a Nylon 0.45 µm sieve Chrodisc syringe filter. Finally, the concentration of the metal ion in the different aqueous solutions was measured by Atomic Absorption Spectroscopy (AAS), using an AA-7000 Shimadzu equipment.

Adsorption kinetic curves were carried out with and adsorbent dosage of 5 g/L, while the initial Co(II) and Li(I) concentrations were kept in 40 mg/L and 20 mg/L, respectively. The kinetic curves were evaluated by filling several Eppendorf tubes with the same ion concentration and solid dosage and measuring the ion concentration at different times. Each point of the kinetic curve was evaluated three times and the average value was used,

to evaluate the uncertainty. The adsorbent capacity and the percentage of adsorbed Co^{2+}, and Li^{+} were obtained by mass balance, employing Equations (1) and (2) respectively [31].

$$q = \frac{C_0 - C}{m} \cdot V \quad (1)$$

$$\%M^{n+}_{Adsorbed} = \frac{C_0 - C}{C_0} \cdot 100 \quad (2)$$

2.3. Adsorption Equilibrium Experiments

The adsorption isotherms were carried out using tubes placed in the same thermo block (Hettich Lab Technology, Tuttlingen, Germany) previously employed, with the same stirring rate, at 298 K. To develop the isotherm, the dose of adsorbent material was kept constant at 1 g/L and ion concentrations were changed from 50 mg/L to 200 mg/L. To ensure the equilibrium was attained, all the tubes were kept stirred at constant temperature for 24 h.

3. Results and Discussion

3.1. Adsorbent Characterization

3.1.1. X-ray Diffraction

Figure 1 shows the XRD results corresponding to NaYBFK and 13XBFK with their corresponding protonated forms. According to the diffractograms, all the zeolites display the typical peaks of the FAU structure [32]. It can also be observed that the diffractograms of the protonated zeolites showed less intense peaks than the corresponding original solids. However, the amorphous halo seems to remain unaltered indicating that the decrease in crystallinity due to acid treatment is relatively small, consequence of the diluted HCl solution employed. Additionally, this decrease in the intensity of the peaks can also be associated with the substitution of cations by H^{+} which have a higher charge to ionic radius ratio, resulting in a less defined diffraction patterns [33].

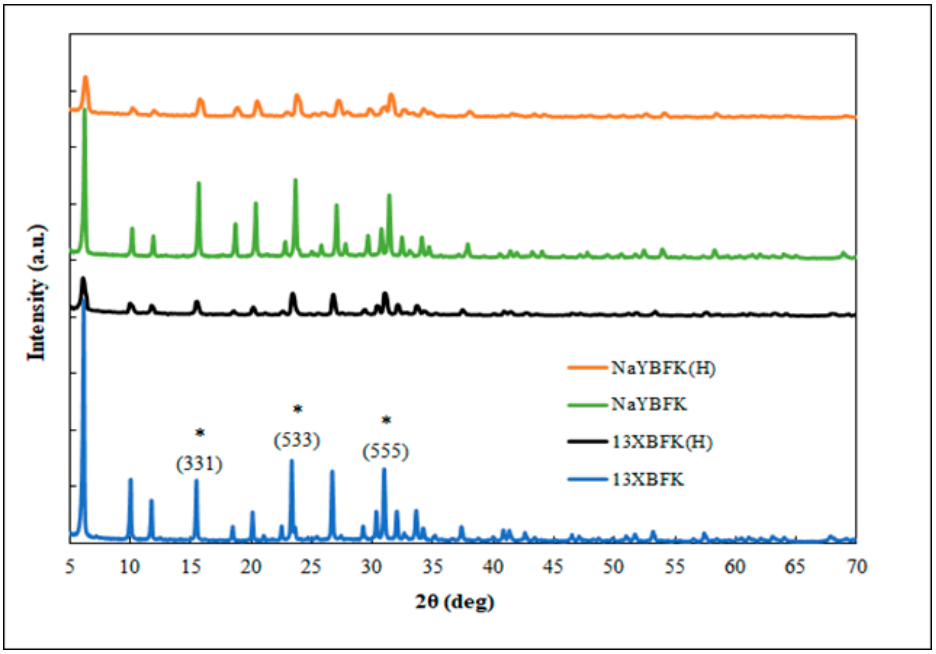

Figure 1. XRD pattern of NaYBFK, NaYBFK(H), 13XBFK and 13XBFK(H).

3.1.2. X-ray Fluorescence

Table 1 shows the results obtained for the elemental composition analysis of the zeolites samples, expressed as oxide percentage. As expected, the higher molar fraction

percentages correspond to Si and Al, which corroborate the aluminum silicate framework of the zeolites. Additionally, the Si/Al ratio gave information about the type of zeolites: although both were FAU framework the X zeolites presented Si/Al molar ratios around 1.2–1.3 (<1.5) whereas for Y zeolites were close to 3 (>1.5). Protonated zeolites presented Si/Al molar ratios higher than non-protonated zeolites which corroborated the partial removal of aluminum by the protonation process.

Table 1. Chemical composition in molar fraction (mol %).

	13XBFK	**13XBFK(H)**	**NaYBFK**	**NaYBFK(H)**
SiO_2	57.48	61.22	74.23	74.87
Al_2O_3	23.37	23.36	13.82	13.50
Na_2O	16.88	12.34	9.81	7.59
MgO	1.57	1.58	1.15	2.30
K_2O	0.07	0.06	0.05	0.05
CaO	0.00	0.14	0.50	0.56
Si/Al molar ratio	1.23	1.31	2.69	2.77
Cations/Al molar ratio	0.79	0.60	0.83	0.78
Protonation degree (%)	21	40	17	22

Theoretically the cation/Al ratio should be close to 1, as the interchangeable cations (Na^+, K^+, Mg^{2+} and Ca^{2+} in this case) appear in the zeolite to balance the mismatch caused by the substitution of a silicon (IV) for an aluminum (III) cation. So, the difference between 1 and this ratio is assumed to be the protonation degree of the zeolites (molar mass of hydronium ion is not heavy enough to be detected by XRF). This fact was also confirmed by 13Al NMR measurements, to discard the existence of extra red aluminum.

As it can be observed, protonation degree was higher in the protonated zeolites, indicating that the treatment carried out has led to an increase in the amount of H^+ cations. However, this increase was greater for X zeolite, achieving an increase up to 40%, while Y zeolite only increased by 5%. The reason of this behavior can be due to the different Si/Al ratio. The Si/Al ratio of X zeolite is lower than the one of Y zeolite. This indicates that X zeolite has more positions to locate the cations which balance the charges and consequently, more easiness to exchange these cations by protons. This exchange capacity allows these materials to be successfully employed as adsorbents.

3.1.3. Isotherms Adsorption–Desorption of N_2

Figure 2 shows the N_2 adsorption-desorption isotherms. According to the IUPAC classification [34], the nitrogen sorption isotherms of the zeolite samples are type II curves, which are characteristic of microporous adsorbents. The shape of the curves is the result of unrestricted mono- and multilayer adsorption up to high p/p_0 values. Gradual curvature at low p/p_0 values indicates overlapping monolayer coverage and initiation of multilayer adsorption in all the cases, apart from 13XBFK solid, which present the steepest slope. On the other hand, an H4 type hysteresis cycle was observed for all the zeolites. This behavior is typical of zeolite aggregates and large external surface area zeolites.

Table 2 displays the textural properties of the materials. It shows the values of the main parameters obtained from the analysis of the isotherms: specific surface BET area (S_{BET}), BET constant (C), external surface area calculated using t-plot method (SEXT), inner surface area (S_{INT}), and micropore volume and average pore diameter calculated with BJH method.

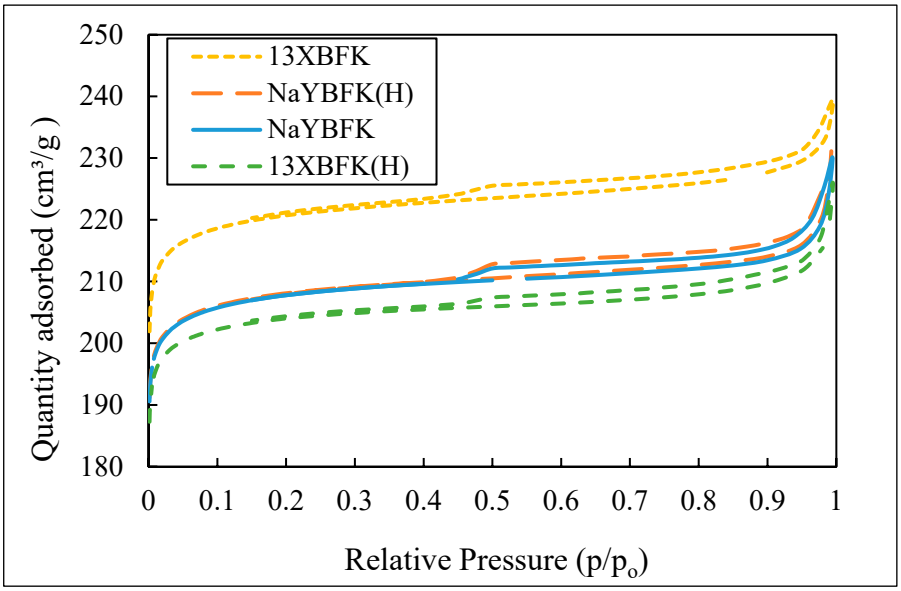

Figure 2. Nitrogen sorption isotherms at 77 K on zeolite samples.

Table 2. Textural parameters of 13XBFK, 13XBFK(H), NaYBFK and NaYBFK(H).

Adsorbent	S_{BET} (m^2/g)	C·10^{-3}	S_{INT} (m^2/g)	S_{EXT} (m^2/g)	Micropore Volume (cm^3/g)	Average Pore Size (Å)
13XBFK	910	18.5	860	50	0.319	16.2
13XBFK(H)	845	20.0	805	40	0.297	16.5
NaYBFK	875	21.2	825	50	0.306	16.6
NaYBFK(H)	860	22.7	810	50	0.301	16.8

The large specific surface area of all zeolites must be highlighted. In all the tested zeolites, the internal surface area was above 800 m^2/g with a similar external surface area. The protonation process slightly decreased the surface area since an increase in Si/Al ratio occurred. Additionally, an acid treatment can dissolve amorphous silica fragment, blocking the channels. However, the reduction in the surface area was practically negligible because it stayed at high values (>840 m^2/g). In relation with the inner surface area, it seems to be independent of the protonation process, as it only varies less than 10%, in agreement with literature [35]. Regarding the micropore volume, the protonated samples had a little less micropore volume and a larger average pore size. This difference could be attributed to the fact that the acid treatment can slightly alter the pore connectivity, because of the exchange of cations by protons. Similar behaviors can be found in literature [36].

3.1.3.1. pH Evolution in Aqueous Suspension of Zeolite Samples

Initially, before carrying out the adsorption tests, the evolution of the pH of the different zeolites in aqueous suspensions, was measured at different times (Figure 3). The evolution of the pH is a key factor to study the adsorption process since Co^{2+} precipitate as hydroxides at pH values higher than 9 [6]. Therefore, it is important to carry out the adsorption experiments at pH values lower than 9 to be sure that adsorption and not precipitation is taking place.

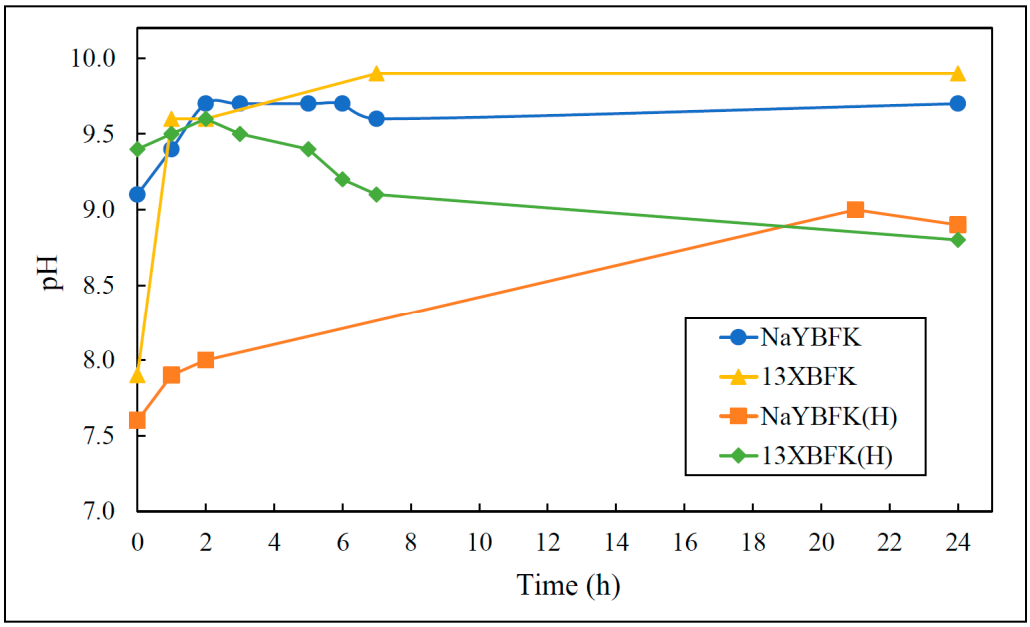

Figure 3. pH measurements of the different adsorbent materials suspended in distilled water over time, with a dose of 1 g/L.

The aqueous suspensions of 13XBFK and NaYBFK zeolites showed a similar behavior: an increase of the pH with the time, achieving a steady value near pH 10. On the other hand, the pH of the suspensions of the protonated zeolites also increased with time, but reaching a final pH value of 9, due to higher protonation degree. The increase in the pH was due to the ionic exchange of the sodium by proton, decreasing its concentration in the aqueous media. According to these results, it can be concluded that only the protonated zeolites could be used for the recovery of these metals. However, when the zeolites are suspended not in distilled water, but in metal solutions, the final pH slightly decreases: 6.0 for cobalt and 6.5 for lithium. Therefore, the raw zeolites as well as the protonated ones could be employed as adsorbents.

3.2. Influence of the Exchanged Cation

To determine the influence of the cation exchanged in the zeolite, cobalt and lithium adsorption experiments were developed employing both NaYBFK and 13XBFK zeolites, as well as their protonated forms. Table 3 displays the adsorption capacity as well as the percentage of metal removed, after 40 min.

Table 3. Adsorption capacities and percentage of metal removed of 13XBFK, 13XBFK(H), NaYBFK and NaYBFK(H).

	13XBFK	**13XBFK(H)**	**NaYBFK**	**NaYBFK(H)**
		Cobalt Adsorption		
q (mg/g)	23.0	17.6	24.2	23.4
% Removed	96.4	99.1	99.3	99.5
		Lithium adsorption		
q (mg/g)	0.30	0.28	0.30	0.30
% Removed	27.4	25.6	26.9	27.4

As it can be observed, the protonation process does not significantly improve the adsorption capacity of the zeolite, which indicates that the decrease in crystallinity and the

increase in Si/Al ratio in protonated forms does not affect the adsorption process. Thus, non-protonated solids were employed in further experiments, to analyze the kinetic curves.

3.3. Kinetic Adsorption Experiments

As it has been mentioned above, kinetic studies were performed using non-protonated NaYBFK and 13XBFK zeolites. The kinetic curves of the metallic solutions are displayed in Figures 4 and 5. It can be observed that the cobalt adsorption capacity of both zeolites is clearly higher than the lithium adsorption capacity. So, both zeolites can remove about 100% of cobalt, but just around 30% of lithium. This indicates that these materials can be employed to successfully separate both ionic species.

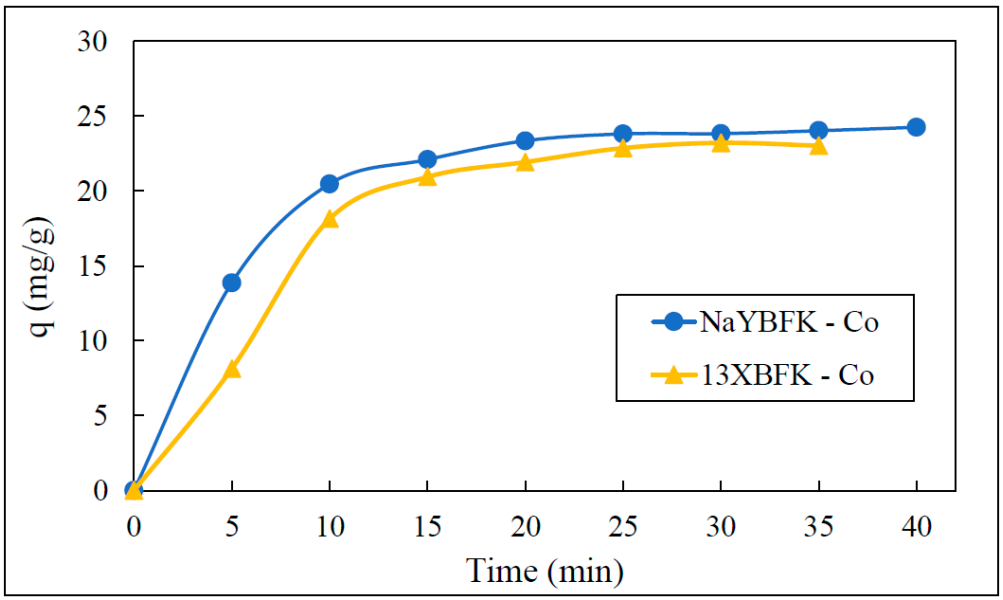

Figure 4. Co^{2+} adsorption at 298 K. Conditions: 5 g/L of adsorbent dosage, 1100 rpm, and 40 mg/L of initial Co^{2+} concentration.

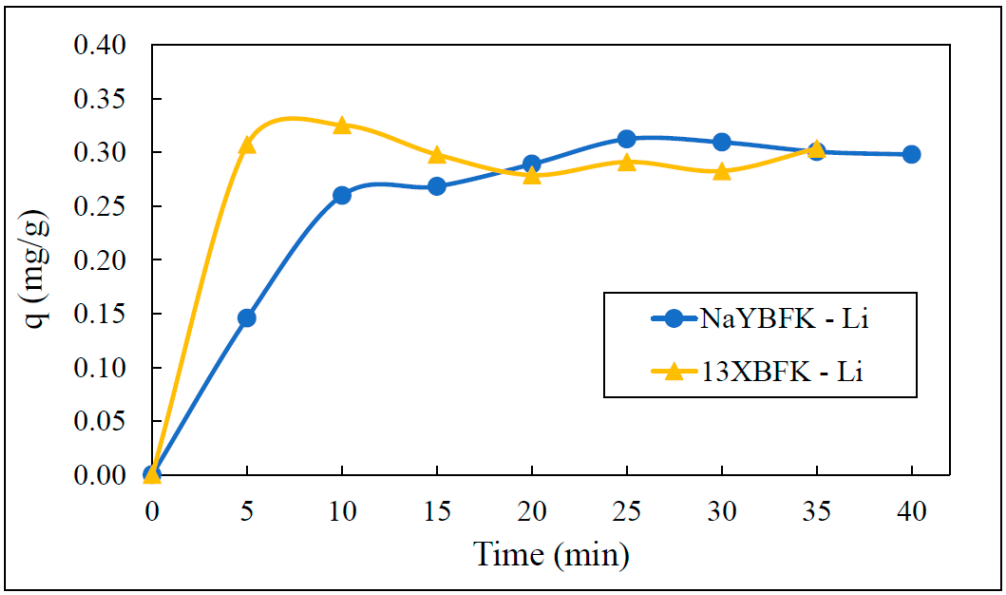

Figure 5. Li^{+} adsorption at 298 K. Conditions: 5 g/L of adsorbent dosage, 1100 rpm, and 20 mg/L of initial Li^{+} concentration.

The different behavior can be discussed in terms of the hydrated ionic radii, dehydration energies, electronegativity, and ionic mobility. The values of these parameters for the three cations are summarized in Table 4. According to literature, the larger the electronegativity, the higher the affinity of the zeolite towards the cation. This fact could explain why the cobalt adsorption capacity are higher than the lithium one [37]. Additionally, the small molecular mass (6.9), low charge and small hydrated ionic radius of lithium reinforces this behavior: the driving force and the electrostatic interaction between the lithium ions and sorption sites will be significantly lower than that of cobalt [38].

Table 4. Properties of Co^{2+} and Li^{+} in aqueous solution.

	Hydrated Ionic Radius (Å) [39]	**Dehydration Energy (kJ/mol)**	**Electronegativity [40]**	**Ionic Mobility (10^{-5} cm^2/s) [41]**
Co^{2+}	4.23	2054	1.88	0.732
Li^{+}	3.82	520	0.98	1.029

The kinetic curves experimentally obtained were analyzed using different kinetics models [42]. Correlation coefficient (R^2) and root mean squared error (RMSE) were employed to analyze the goodness of the adjustments.

Pseudo-first-order kinetic model or Lagergren equation is one of the most widely used models and it was the first-rate equation developed for sorption in liquid/solid systems [43].

$$\ln(q_e - q) = lnq_e - k_1 \cdot t \quad (3)$$

where q and q_e are the amounts of Co^{2+} adsorbed onto the adsorbent at time t and at equilibrium time (mg/g), respectively, and k_1 is the constant rate of first order (min^{-1}).

Pseudo-second-order kinetic model, [44], is employed to determine the amount of metal adsorbed on the zeolite by the model expressed as:

$$\frac{t}{q} = \frac{1}{k_2 \cdot q_e^2} + \frac{t}{q_e} \quad (4)$$

where k_2 is the constant rate of second order (min·g/mg). If second-order kinetic model is applicable, the plot of t/q against t should show a linear trend. The value q_e can be determined from the slope of this plot, so this model predicts the behavior over the whole range of adsorption if there are not diffusional limitations to the adsorption.

The determined kinetic parameters obtained after fitting the experimental data to the different models are displayed in Table 5. To ascertain the goodness of the fittings, R^2 correlation coefficient, RMSE and F-values were calculated with Microsoft Excel®. So, the more adequate model will be the one with higher correlation coefficient, low value of RSME and, according to literature, the one with the larger F-value [45]. Although the correlation coefficient is similar in both pseudo-first order and pseudo-second order model, the RMSE value is clearly lower in the second case. Thus, attending to the statistical parameters, it can be concluded that the kinetic model which best represents the phenomenon is the pseudo-second order model. The pseudo-second order model implies the nonexistence of diffusional limitations to the adsorption, which is expected in this case, because of the difference between the material average pore size and the hydrated ions size [26]. Therefore, the adsorption mechanism is controlled by the adsorption step and the external and internal mass transfer resistances do not affect the overall process.

Table 5. Kinetic parameters for Co^{2+} and Li^{+} adsorption on NaYBFK and 13XBFK.

NaYBFK Adsorbent					
Pseudo-First Order					
Cation	q_e (mg/g)	k_1 (min^{-1})	R^2	RMSE	F value
Co(II)	24.09	0.176	0.999	0.459	1.004
Li(I)	0.31	0.150	0.988	0.001	1.034
Pseudo-second order					
Cation	q_e (mg/g)	k_2 (g·min/mg)	R^2	RMSE	F value
Co(II)	27.74	0.008	0.992	3.47	0.998
Li(I)	0.37	0.449	0.973	0.002	0.997
13XBFK adsorbent					
Pseudo-first order					
Cation	q_e (mg/g)	k_1 (min^{-1})	R^2	RMSE	F value
Co(II)	23.92	0.119	0.981	10.4012	1.094
Li(I)	0.31	0.430	0.957	0.004	0.948
Pseudo-second order					
Cation	q_e (mg/g)	k_2 (g·min/mg)	R^2	RMSE	F value
Co(II)	30.55	0.0037	0.966	17.72	1.081
Li(I)	0.30	$5.58.10^4$	0.981	0.001	1.019

To further analyze the adsorption mechanism, the kinetic data were adjusted to Webber-Morris intraparticle diffusion model [46], described by Equation (5), to ascertain if there is intraparticle or boundary layer diffusion. In this equation, *C* is the intersection to the ordinate axis, k_i (mg/g·$min^{1/2}$) indicates the intraparticle diffusion rate constant, and q_e and q represent the adsorption capacities at equilibrium and at t time, respectively (mg/g). The Webber-Morris plots are displayed in Figures 6 and 7.

$$q = k_i \cdot t^{\frac{1}{2}} + C \quad (5)$$

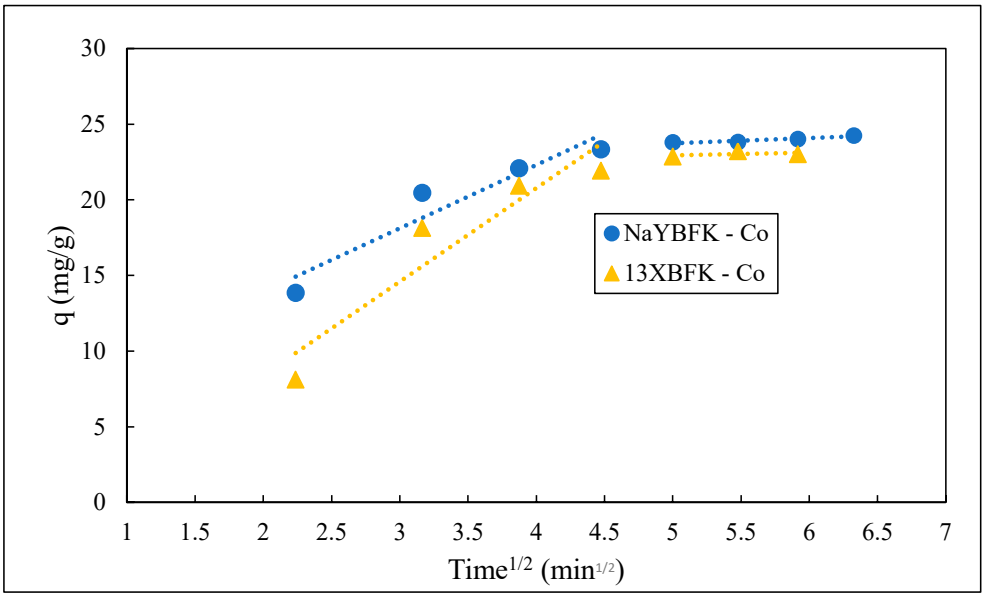

Figure 6. Webber-Morris plot for Co^{2+} adsorption at 298 K. Conditions: 5 g/L of adsorbent dosage, 1100 rpm, and 40 mg/L of initial Co^{2+} concentration.

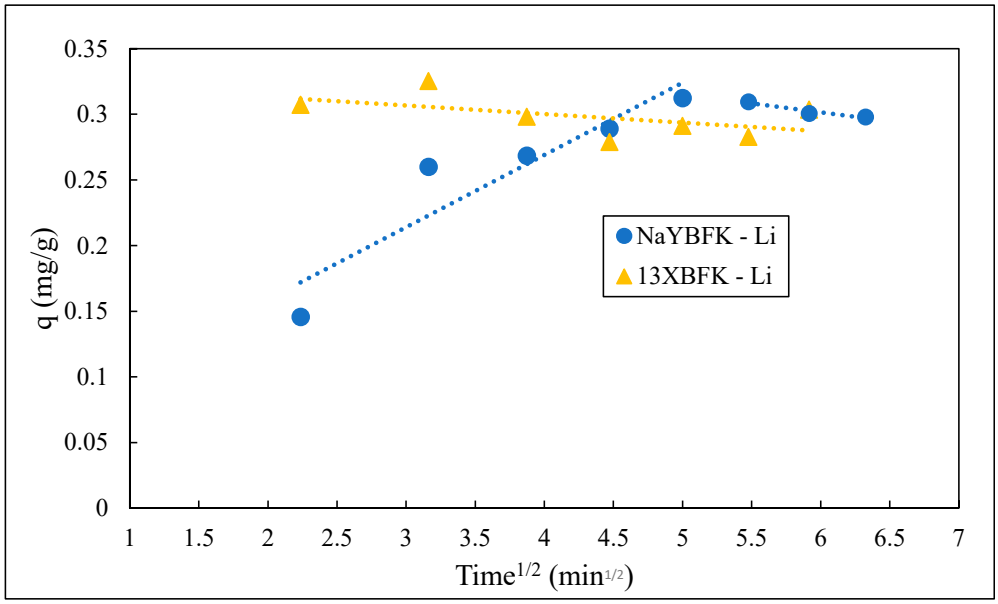

Figure 7. Webber-Morris plot for Li^+ adsorption at 298 K. Conditions: 5 g/L of adsorbent dosage, 1100 rpm, and 20 mg/L of initial Li^+ concentration.

As it can be observed in Webber-Morris plots, except for the case of lithium adsorption onto 13XBFK, all the plots can be divided in two linear sections. The first one corresponds to the diffusion of ions though the external surface of the adsorbent (film diffusion), while the second one corresponds to intraparticle diffusion. In the case of lithium adsorption onto 13XBFK only a straight line is observed: this indicates that in this case only intraparticle diffusion is noticeable. Additionally, none of the curves cross the origin which implies that, according to this model [46], the intraparticle diffusion, although important, is not the rate-limiting step in the adsorption process. So, the rate-limiting step is the adsorption process, in agreement with pseudo-second-order model assumption.

3.4. Kinetic Equilibrium Experiments

To describe the nature of the adsorption interactions the isotherms of cobalt and lithium ions on 13XBFK zeolite were carried out. According to Giles classification, the adsorption isotherms displayed in Figure 8 can be classified as H1 (for Li^+) and H2 (for Co^{2+}) types [47]. These involve power functions which can be derived from continuous site–affinity distributions. To further analyze the adsorption isotherms, the experimental data were fitted to Langmuir and Freundlich models, as they are the most adequate models for this kind of isotherms. The fitting isotherm parameters obtained for each temperature are shown in Table 6, along with the correlation coefficients and (RMSE).

Langmuir model is described in Equation (6), where, q_{sat} (mg/g) indicates the maximum capacity of adsorption on the monolayer and b (L/mg) is a constant related to the affinity between adsorbent and adsorbate.

$$q_e = \frac{q_{sat} \cdot b \cdot C_e}{1 + b \cdot C_e} \quad (6)$$

Freundlich model is described in Equation (7), where, K_F (L/mg) and n are characteristic parameters of the model. The value 1/n is an empirical constant that informs about the strength of the adsorption process and the surface heterogeneity

$$q_e = K_F \cdot C_e^{1/n} \quad (7)$$

As it can be observed in Figure 6, both isotherm models fit relatively well to the experimental data. This is confirmed by the similar values of the R^2 coefficients. In the

case of cobalt, although Freundlich adjustment present smaller RMSE value, it seems that Langmuir model correctly represents the behavior of the adsorption process, as it perfectly predicts the experimental saturation capacity. Regarding lithium adsorption, it seems that the best model to reproduce this phenomenon is Freundlich equation. This model is typical of heterogeneous adsorbent surfaces with different adsorption sites, and of solids which do not have a finite saturation capacity, what it is observed here. Additionally, according to the statistical theory of adsorption value of 1/n in the adsorption isotherm less than unity implies heterogeneous surface structure with minimum interactions between the adsorbed atoms [48]. This behavior is observed in this case.

The results obtained in this manuscript were compared with those previously reported for these metal ions and similar materials (Table 7). As can be observed in this table, the values of saturation capacity for the zeolite used in this study are in the same range or above with the previously reported ones, excepting the composite of Fe_3O_4 and zeolitic imidazole framework, which had a huge adsorption capacity. As for Li, the literature is not very extensive, but the results obtained are very promising.

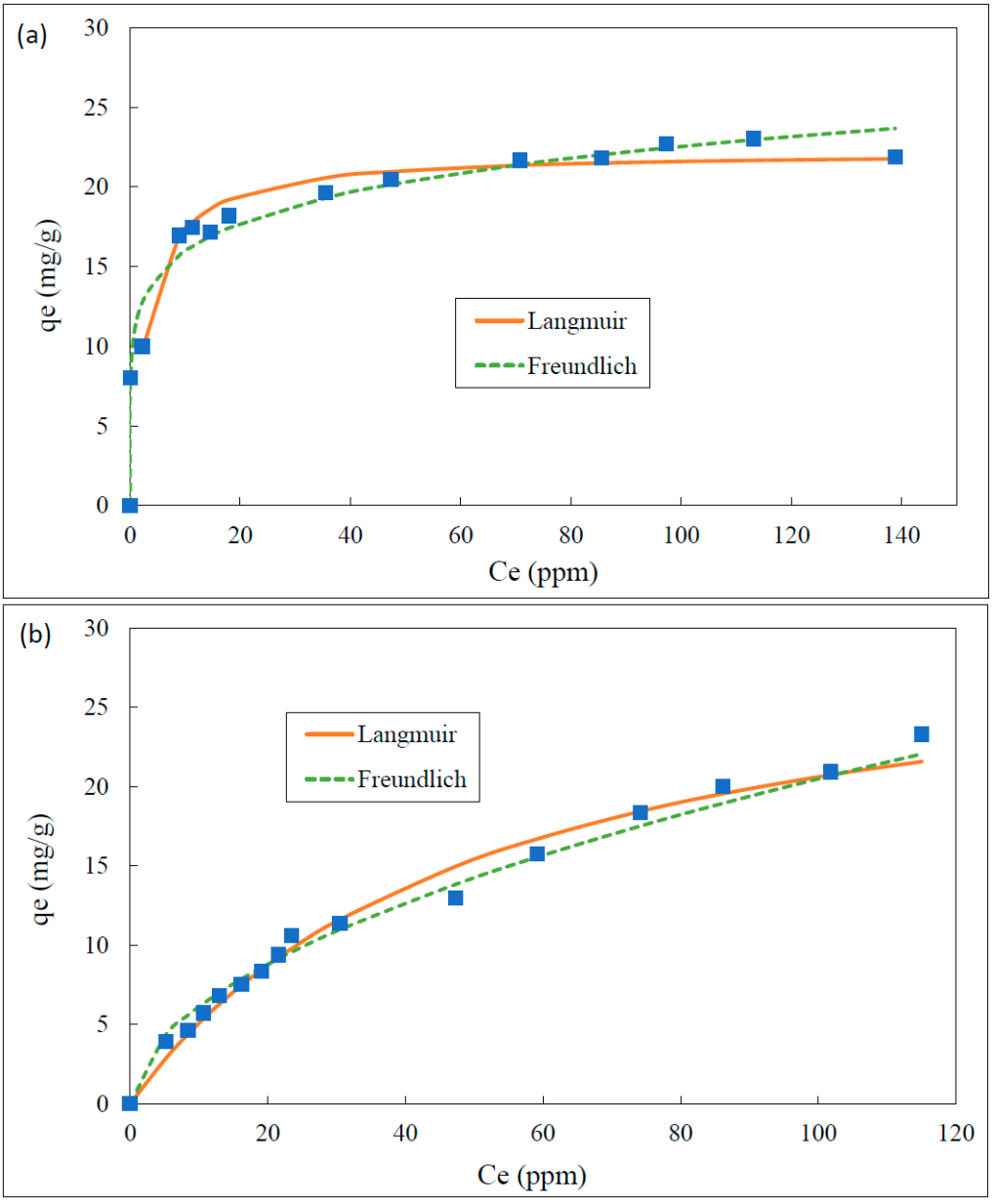

Figure 8. Cobalt (**a**) and lithium (**b**) adsorption isotherms at 25 °C using 13XBFK.

Table 6. Isotherm parameters for Co^{2+} and Li^{+} adsorption on NaYBFK and 13XBFK.

Langmuir Model				
Metal	**q_{sat} (mg/g)**	**b (L/mg)**	**R^2**	**RMSE**
Co(II)	22.12	0.354	0.933	7.7
Li(I)	31.12	0.019	0.987	11.1
Freundlich Model				
Metal	**K_F (L/mg)**	**n**	**R^2**	**RMSE**
Co(II)	11.30	6.67	0.974	14.9
Li(I)	1.82	1.90	0.984	12.7

Table 7. Comparison between literature and the most significative results obtained in the current work.

Reference	**Metal**	**Adsorbent**	**$[Metal]_{Initial}$ (mg/L)**	**Sorbent Dosage (g/L)**	**q_{sat} (mg/g)**
This work	Co	Zeolite X	50	5	22.16
[30]	Co	Clinoptilolite	10–200	12	4.2
[49]	Co	FAU type zeolite synthesized from coal fly ash	100–500	5	12.2
[50]	Co	Composite of Fe_3O_4 and zeolitic imidazole framework 8	5–100	2	71.2
This work	Li	Zeolite X	20	5	0.30
[8]	Li	Lithium—Aluminum hydroxide	350	≈ 0,1	0.6
[51]	Li	Modified cellulose	140	20	16.0
[52]	Li	Manganese oxide	35	0.5	10.9

4. Conclusions

This study has shown that both, NaYBFK and 13XBFK are effective adsorbents to selectively remove cobalt from synthetic wastewater, as it can preferably adsorb cobalt ions vs. lithium ones.

Characterization of the samples has shown that the zeolites treated with acid have suffered a slightly dealumination process which has contributed to a Si/Al ratio increase and therefore a reduction in the number of exchangeable cations. Also, as it is shown in BET results, the protonation of zeolites increases the BET surface: protons are smaller than sodium cations, so the structure of zeolite channels is more accessible for N_2 penetration. Consequently, it involves a decrease in the crystallinity as it is shown on XRD plot (Figure 1).

The adsorption kinetics follow a pseudo-second order model in all the cases. Additionally, kinetic results indicate that using both zeolites it is possible to remove about 100% of cobalt from aqueous solutions at 40 min, meanwhile just around 30% of lithium is removed, what implies a separation factor of 3.33. This selectivity is important as these two metals frequently appear together in leaching solutions from, for example, ion-Li batteries.

Regarding adsorption equilibrium, Langmuir model is perfectly capable of predicting the experimental cobalt saturation capacity, while Freundlich model is the most adequate to represent lithium adsorption as this process does not have finite saturation capacity.

To sum up, NaYBFK and 13XBFK are commercial and cost-effective adsorbent that have good properties for the selective removal of cobalt from water, which is important as this cation usually appears in wastewaters along with other cations, as lithium, towards which the zeolites have much less adsorption capacity. Afterwards, once the two metals are selectively separated, they could be recovered by means of other techniques, such as solvent extraction or precipitation.

Author Contributions: E.D.: data curation, formal analysis, writing—original draft, writing—review & editing funding acquisition. C.R.: investigation, methodology, writing—original draft. J.M.G.: formal analysis, data curation, funding acquisition. R.M.: writing—review & editing. A.R.: formal analysis, writing—review & editing, resources, funding acquisition All authors have read and agreed to the published version of the manuscript.

Funding: This work was supported by the financial support of the Santander-UCM 2020 project [PR108/20-07]; and by a contract of research assistant from the Community of Madrid to C.R. through the program "Garantía Juvenil" [CT103/19/PEJ-2019-AI/IND-13004].

Data Availability Statement: Not applicable.

Acknowledgments: Authors are grateful to the UCM research support centers (CAIs) for the XRD and XRF analyses, and Chemiewerk Bad Köstritz GmbH for the supply of the zeolites.

Conflicts of Interest: The authors declare no conflict of interest.

References

1. Burakov, A.E.; Galunin, E.V.; Burakova, I.V.; Kucherova, A.E.; Agarwal, S.; Tkachev, A.G.; Gupta, V.K. Adsorption of heavy metals on conventional and nanostructured materials for wastewater treatment purposes: A review. *Ecotoxicol. Environ. Saf.* **2018**, *148*, 702–712. [CrossRef] [PubMed]
2. Hu, W.; Lu, S.; Song, W.; Chen, T.; Hayat, T.; Alsaedi, N.S.; Chen, C.; Liu, H. Competitive adsorption of U(VI) and Co(II) on montmorillonite: A batch and spectroscopic approach. *Appl. Clay Sci.* **2018**, *157*, 121–129. [CrossRef]
3. Islam, M.A.; Morton, D.W.; Johnson, B.B.; Pramanik, B.K.; Mainali, B.; Angove, M.J. Opportunities and constraints of using the innovative adsorbents for the removal of cobalt(II) from wastewater: A review. *Environ. Nanotechnol. Monit. Manag.* **2018**, *10*, 435–456. [CrossRef]
4. Lemaire, J.; Svecova, L.; Lagallarde, F.; Laucournet, R.; Thivel, P.X. Lithium recovery from aqueous solution by sorption/desorption. *Hydrometallurgy* **2014**, *143*, 1–11. [CrossRef]
5. Coman, V.; Robotin, B.; Ilea, P. Nickel recovery/removal from industrial wastes: A review. *Resour. Conserv. Recycl.* **2013**, *73*, 229–238. [CrossRef]
6. Chivot, J.; Mendoza, L.; Mansour, C.; Pauporté, T.; Cassir, M. New insight in the behaviour of Co-H_2O system at 25–150 °C, based on revised Pourbaix diagrams. *Corros. Sci.* **2008**, *50*, 62–69. [CrossRef]
7. Kyzas, G.Z.; Deliyanni, E.A.; Matis, K.A. Activated carbons produced by pyrolysis of waste potato peels: Cobaltions removal by adsorption. *Colloids Surf. A Physicochem. Eng. Asp.* **2016**, *490*, 74–83. [CrossRef]
8. Jiang, H.; Yang, Y.; Sun, S.; Yu, J. Adsorption of lithium ions on lithium-aluminum hydroxides: Equilibrium and kinetics. *Can. J. Chem. Eng.* **2020**, *98*, 544–555. [CrossRef]
9. Purnomo, C.W.; Kesuma, E.P.; Perdana, I.; Aziz, M. Lithium recovery from spent Li-ion batteries using coconut shell activated carbon. *Waste Manag.* **2018**, *79*, 454–461. [CrossRef]
10. Pahlavanzadeh, H.; Motamedi, M. Adsorption of nickel, Ni(ii), in aqueous solution by modified zeolite as a cation-exchange adsorbent. *J. Chem. Eng. Data* **2020**, *65*, 185–197. [CrossRef]
11. Blengini, G.A.; Latunussa, C.E.L.; Eynard, U. Study on the EU's List of Critical Raw Materials—Critical Raw Materials Factsheets. European Commission: Brussels, Belgium, 2020. Available online: https://op.europa.eu/en/publication-detail/-/publication/c0d5292a-ee54-11ea-991b-01aa75ed71a1/language-en (accessed on 7 December 2022).
12. Xu, J.; Thomas, H.R.; Francis, R.W.; Lum, K.R.; Wang, J.; Liang, B. A review of processes and technologies for the recycling of lithium-ion secondary batteries. *J. Power Sources* **2008**, *177*, 512–527. [CrossRef]
13. Karate, V.D.; Marathe, K.V. Simultaneous removal of nickel and cobalt from aqueous stream by cross flow micellar enhanced ultrafiltration. *J. Hazard. Mater.* **2008**, *157*, 464–471. [CrossRef] [PubMed]
14. Barakat, M.A. New trends in removing heavy metals from industrial wastewater. *Arab. J. Chem.* **2011**, *4*, 361–377. [CrossRef]
15. Assaad, E.; Azzouz, A.; Nistor, D.; Ursu, A.V.; Sajin, T.; Miron, D.N.; Monette, F.; Niquette, P.; Hausler, R. Metal removal through synergic coagulation-flocculation using an optimized chitosan-montmorillonite system. *Appl. Clay Sci.* **2007**, *37*, 258–274. [CrossRef]
16. Demirbaş, E. Adsorption of cobalt(II) ions from aqueous solution onto activated carbon prepared from hazelnut shells. *Adsorpt. Sci. Technol.* **2003**, *21*, 951–963. [CrossRef]
17. Sari, A.; Tüzen, M. Adsorption of silver from aqueous solution onto raw vermiculite and manganese oxide-modified vermiculite. *Microporous Mesoporous Mater.* **2013**, *170*, 155–163. [CrossRef]
18. Sari, A.; Tuzen, M. Cd(II) adsorption from aqueous solution by raw and modified kaolinite. *Appl. Clay Sci.* **2014**, *88–89*, 63–72. [CrossRef]
19. Saleh, T.A.; Sari, A.; Tuzen, M. Chitosan-modified vermiculite for As(III) adsorption from aqueous solution: Equilibrium, thermodynamic and kinetic studies. *J. Mol. Liq.* **2016**, *219*, 937–945. [CrossRef]
20. Saleh, T.A.; Sarı, A.; Tuzen, M. Effective adsorption of antimony(III) from aqueous solutions by polyamide-graphene composite as a novel adsorbent. *Chem. Eng. J.* **2017**, *307*, 230–238. [CrossRef]

21. Tuzen, M.; Saleh, T.A.; Sarı, A. Naeemullah Interfacial polymerization of trimesoyl chloride with melamine and palygorskite for efficient uranium ions ultra-removal. *Chem. Eng. Res. Des.* **2020**, *159*, 353–361. [CrossRef]
22. Prabakaran, R.; Arivoli, S. Removal of cobalt (II) from aqueous solutions by adsorption on low cost activated carbon. *Int. J. Sci. Eng. Technol. Res.* **2013**, *2*, 271–283.
23. Kobya, M.; Demirbas, E.; Senturk, E.; Ince, M. Adsorption of heavy metal ions from aqueous solutions by activated carbon prepared from apricot stone. *Bioresour. Technol.* **2005**, *96*, 1518–1521. [CrossRef] [PubMed]
24. Deravanesiyan, M.; Beheshti, M.; Malekpour, A. Alumina nanoparticles immobilization onto the NaX zeolite and the removal of Cr (III) and Co(II) ions from aqueous solutions. *J. Ind. Eng. Chem.* **2015**, *21*, 580–586. [CrossRef]
25. Wang, H.; Huang, K.; Zhang, Y.; Chen, X.; Jin, W.; Zheng, S.; Zhang, Y.; Li, P. Recovery of Lithium, Nickel, and Cobalt from Spent Lithium-Ion Battery Powders by Selective Ammonia Leaching and an Adsorption Separation System. *ACS Sustain. Chem. Eng.* **2017**, *5*, 11489–11495. [CrossRef]
26. Díez, E.; Gómez, J.M.; Rodríguez, A.; Bernabé, I.; Sáez, P.; Galán, J. A new mesoporous activated carbon as potential adsorbent for effective indium removal from aqueous solutions. *Microporous Mesoporous Mater.* **2020**, *295*, 109984. [CrossRef]
27. Li, H.; Zheng, F.; Wang, J.; Zhou, J.; Huang, X.; Chen, L.; Hu, P.; Gao, J.M.; Zhen, Q.; Bashir, S.; et al. Facile preparation of zeolite-activated carbon composite from coal gangue with enhanced adsorption performance. *Chem. Eng. J.* **2020**, *390*, 124513. [CrossRef]
28. Iftekhar, S.; Heidari, G.; Amanat, N.; Zare, E.N.; Asif, M.B.; Hassanpour, M.; Lehto, V.P.; Sillanpaa, M. Porous materials for the recovery of rare earth elements, platinum group metals, and other valuable metals: A review. *Environ. Chem. Lett.* **2022**, *20*, 3697–3746. [CrossRef]
29. Araissi, M.; Elaloui, E.; Moussaou, Y. The removal of Cadmium, Cobalt, and Nickel by adsorption with Na-Y zeolite. *Iran. J. Chem. Chem. Eng.* **2020**, *39*, 169–179.
30. Rodríguez, A.; Sáez, P.; Díez, E.; Gómez, J.M.; García, J.; Bernabé, I. Highly efficient low-cost zeolite for cobalt removal from aqueous solutions: Characterization and performance. *Environ. Prog. Sustain. Energy* **2019**, *38*, S352–S365. [CrossRef]
31. Conte, N.; Gómez, J.M.; Díez, E.; Sáez, P.; Monago, J.I.; Espinosa, A.; Rodríguez, A. Sequential separation of cobalt and lithium by sorption: Sorbent set selection. *Sep. Purif. Technol.* **2022**, *303*, 122199. [CrossRef]
32. Treacy, M.M.J.; Higgins, J.B. Collection of Simulated XRD Powder Patterns for Zeolites, 5th ed.Elsevier Science: Amsterdam, The Netherland, 2007; ISBN 0144-2449.
33. Kennedy, D.A.; Tezel, F.H. Cation exchange modification of clinoptilolite—Screening analysis for potential equilibrium and kinetic adsorption separations involving methane, nitrogen, and carbon dioxide. *Microporous Mesoporous Mater.* **2018**, *262*, 235–250. [CrossRef]
34. Thommes, M.; Kaneko, K.; Neimark, A.V.; Olivier, J.P.; Rodriguez-Reinoso, F.; Rouquerol, J.; Sing, K.S.W. Physisorption of gases, with special reference to the evaluation of surface area and pore size distribution (IUPAC Technical Report). *Pure Appl. Chem.* **2015**, *87*, 1051–1069. [CrossRef]
35. Lanzafame, P.; Papanikolaou, G.; Perathoner, S.; Centi, G.; Migliori, M.; Catizzone, E.; Giordano, G. Reassembly mechanism in Fe-Silicalite during NH4OH post-treatment and relation with the acidity and catalytic reactivity. *Appl. Catal. A Gen.* **2019**, *580*, 186–196. [CrossRef]
36. Garcia-Basabe, Y.; Rodriguez-Iznaga, I.; De Menorval, L.C.; Llewellyn, P.; Maurin, G.; Lewis, D.W.; Binions, R.; Autie, M.; Ruiz-Salvador, A.R. Step-wise dealumination of natural clinoptilolite: Structural and physicochemical characterization. *Microporous Mesoporous Mater.* **2010**, *135*, 187–196. [CrossRef]
37. Arshadi, M.; Amiri, M.J.; Mousavi, S. Kinetic, equilibrium and thermodynamic investigations of Ni(II), Cd(II), Cu(II) and Co(II) adsorption on barley straw ash. *Water Resour. Ind.* **2014**, *6*, 1–17. [CrossRef]
38. Füger, A.; Konrad, F.; Leis, A.; Dietzel, M.; Mavromatis, V. Effect of growth rate and pH on lithium incorporation in calcite. *Geochim. Cosmochim. Acta* **2019**, *248*, 14–24. [CrossRef]
39. Nightingale, E.R. Phenomenological Theory of Ion Solvation. Effective Radii of Hydrated Ions. *J. Phys. Chem.* **1959**, *63*, 1381–1387. [CrossRef]
40. Allred, A.L. Electronegativity values from thermochemical data. *J. Inorg. Nucl. Chem.* **1961**, *17*, 215–221. [CrossRef]
41. Monroe, C.W. Ionic Mobility and Diffusivity. In *Encyclopedia of Applied Electrochemistry*; Kreysa, G., Savinell, R.F., Ota, K., Eds.; Springer: New York, NY, USA, 2014; pp. 1125–1130. ISBN 9781441969958.
42. Simonin, J.P. On the comparison of pseudo-first order and pseudo-second order rate laws in the modeling of adsorption kinetics. *Chem. Eng. J.* **2016**, *300*, 254–263. [CrossRef]
43. Lagergren, S. About the theory of so-called adsorption of soluble substances. *K. Sven. Vetensk. Handl.* **1898**, *24*, 1–39.
44. Ho, Y.S.; McKay, M. Pseudo-second order model for sorption processes. *Process Biochem.* **1999**, *34*, 451–465. [CrossRef]
45. Vuono, D.; Catizzone, E.; Aloise, A.; Policicchio, A.; Agostino, R.G.; Migliori, M.; Giordano, G. Modelling of adsorption of textile dyes over multi-walled carbon nanotubes: Equilibrium and kinetic. *Chin. J. Chem. Eng.* **2017**, *25*, 523–532. [CrossRef]
46. Webber, W.J.; Morris, J.C. Kinetics of Adsorption on Carbon from Solution. *J. Sanit. Eng. Div.* **1963**, *89*, 31–59. [CrossRef]
47. Hinz, C. Description of sorption data with isotherm equations. *Geoderma* **2001**, *99*, 225–243. [CrossRef]
48. Abou-Mesalam, M.M. Applications of inorganic ion exchangers: II—Adsorption of some heavy metal ions from their aqueous waste solution using synthetic iron(III) titanate. *Adsorption* **2004**, *10*, 87–92. [CrossRef]

49. Joseph, I.V.; Tosheva, L.; Doyle, A.M. Simultaneous removal of Cd(II), Co(II), Cu(II), Pb(II), and Zn(II) ions from aqueous solutions via adsorption on FAU-type zeolites prepared from coal fly ash. *J. Environ. Chem. Eng.* **2020**, *8*, 103895. [CrossRef]
50. Kuwer, P.; Yadav, A.; Labhasetwar, P.K. Adsorption of cupric, cadmium and cobalt ions from the aqueous stream using the composite of iron (II,III) oxide and zeolitic imidazole framework-8. *Water Sci. Technol.* **2021**, *84*, 2288–2303. [CrossRef]
51. Xu, C.; Yu, T.; Peng, J.; Zhao, L.; Li, J.; Zhai, M. Efficient adsorption performance of lithium ion onto cellulose microspheres with sulfonic acid groups. *Quantum Beam Sci.* **2020**, *4*, 6. [CrossRef]
52. Wajima, T.; Munakata, K.; Uda, T. Adsorption behavior of lithium from seawater using manganese oxide adsorbent. *Plasma Fusion Res.* **2012**, *7*, 5–8. [CrossRef]